NANO LETTERS

pubs.acs.org/NanoLett Letter

Fracture and Fatigue of Al_2O_3-Graphene Nanolayers

Maedeh Amirmaleki,† Teng Cui,† Yang Zhao, Jason Tam, Anukalp Goel, Yu Sun, Xueliang Sun,* and Tobin Filleter*

Cite This: *Nano Lett.* 2021, 21, 437−444 Read Online

ACCESS | Metrics & More | Article Recommendations | Supporting Information

ABSTRACT: Al_2O_3-graphene nanolayers are widely used within integrated micro/nanoelectronic systems; however, their lifetimes are largely limited by fracture both statically and dynamically. Here, we present a static and fatigue study of thin (1−11 nm) free-standing Al_2O_3-graphene nanolayers. A remarkable fatigue life of greater than one billion cycles was obtained for films <2.2 nm thick under large mean stress levels, which was up to 3 orders of magnitude longer than that of its thicker (11 nm) counterpart. A similar thickness dependency was also identified for the elastic and static fracture behavior, where the enhancement effect of graphene is prominent only within a thickness of ∼3.3 nm. Moreover, plastic deformation, manifested by viscous creep, was observed and appeared to be more substantial for thicker films. This study provides mechanistic insights on both the static and dynamic reliability of Al_2O_3-graphene nanolayers and can potentially guide the design of graphene-based devices.

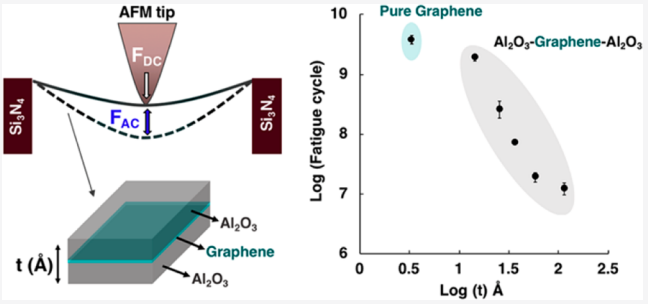

KEYWORDS: *Fatigue, Graphene, Alumina, Mechanical behavior*

INTRODUCTION

Nanoscale amorphous alumina (a-Al_2O_3) films exhibit remarkable mechanical and optical properties,[1−3] high dielectric constant (high-κ),[4] chemical stability, and corrosion resistivity[5,6] and show great promise for a new generation of devices, including flexible electronics, microelectromechanical systems (MEMS), bio-MEMS, battery technologies, and organic permeation barriers.[7−14] Alumina, however, has inherent mechanical limitations as it is generally brittle and exhibits limited room-temperature flexibility. These can be overcome by the integration of graphene, which exhibits excellent electrical, thermal, optical, and mechanical properties.[15−18] The structural and functional combination of alumina and graphene has been applied to a variety of applications, such as high-κ top-gated dielectrics, flexible radio frequency graphene transistors, and pressure sensors.[19−25] Within those optoelectronic and mechanical applications, the devices usually require ultrathin (<10 nm), uniform, and conformable coatings of alumina films to improve the device performance and reliability through techniques such as atomic layer deposition (ALD).[23−25]

The nanoscale Al_2O_3/graphene films in those aforementioned devices are inherently subjected to static and dynamic mechanical stresses, especially with the ever-growing trend of flexible applications. Static failure of nanofilms, for example, may occur under localized stress or as the result of high-stress shocks. Meanwhile, fatigue can also occur under repeated loading when devices are in service.[26] Investigating the fracture and fatigue behavior, and understanding the underlying failure mechanism and size effects on such behavior is critical for designing durable materials and devices. Toward this end, contradictory experimental results have been reported on nanoscale amorphous alumina films, with both fully brittle[27−31] and ductile[32,33] failure being evidenced at room temperature. Moreover, previous studies have investigated the fatigue behavior of thin (4.2 to 50 nm) alumina deposited on silicon substrates and highlighted the cyclic effect on the crack initiation and propagation.[34,35] Meanwhile, approaches to improve these properties are limited in the reported literature, and the effect of graphene on their fatigue life remains unknown. Recently graphene has been reported to exhibit over one billion cycles of fatigue life at high-stress ranges,[36] suggesting that it may contribute to enhance the fatigue response of alumina films. Herein, for the first time, we have studied the fatigue behavior of free-standing a-Al_2O_3@G nanofilms using a modified atomic force microscopy (AFM) testing technique. The elastic and fracture behavior of a-Al_2O_3@G nanofilms were also investigated, and a clear size effect on both the static and fatigue behavior was revealed.

Received: September 24, 2020
Revised: December 21, 2020
Published: December 29, 2020

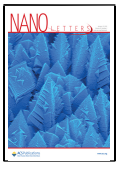

https://dx.doi.org/10.1021/acs.nanolett.0c03868
Nano Lett. 2021, 21, 437−444

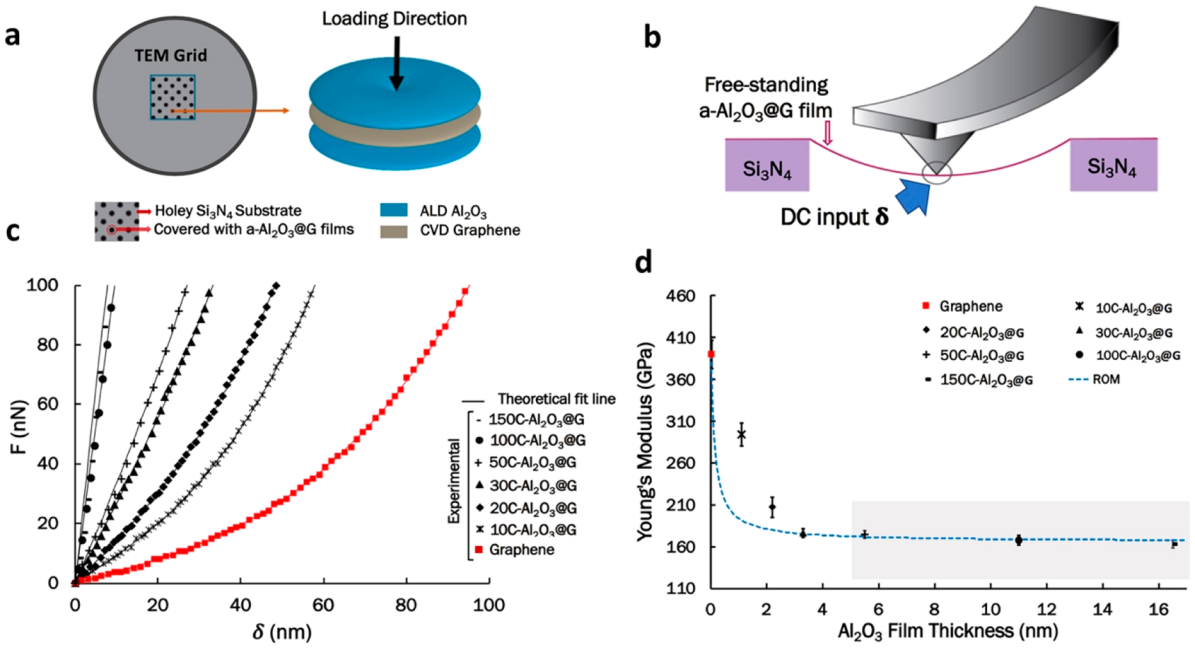

Figure 1. (a) Schematic of a holey TEM grid window with suspended graphene. Al_2O_3 was deposited on both sides of graphene, (b) schematic of AFM deflection testing where a static force is applied at the center of the film, (c) representative $F-\delta$ curves of graphene and a-Al_2O_3@G films of different thickness. Lines represent fitting the data using eq S1, and (d) Young's modulus versus alumina film thickness. The moduli of a-Al_2O_3@G films were in reasonable agreement with ROM above ~3.3 nm with an estimated bulk value of 166 GPa. The gray band shows the range of E values of alumina films of 5−200 nm presented in Table S1.[27−29,38,39,41−43]

RESULTS AND DISCUSSIONS

1. Static Elastic and Fracture Behavior. A series of Al_2O_3 films with the thicknesses of 1.1, 2.2, 3.3, 5.5, 11, and 16.5 nm (using 10, 20, 30, 50, 100, and 150 ALD cycles at 120 °C) were deposited onto monolayer graphene for mechanical characterization (details in SI section 1). ALD method was selected to deposit high-quality alumina films with nanoscale thickness control and high conformality.[37] For simplicity, the films prepared with different ALD cycles were referred to as 10C-Al_2O_3@G, 20C-Al_2O_3@G, 30C-Al_2O_3@G, 50C-Al_2O_3@G, 100C-Al_2O_3@G, and 150C-Al_2O_3@G, with the number before the letter "C" referring to the number of ALD cycles, and "a-Al_2O_3@G" was used when referring to amorphous alumina/graphene nanofilms in general. Chemical vapor deposited (CVD) graphene covering a holey (diameter: 2.7 μm) transmission electron microscopy (TEM) grid was used as a substrate for Al_2O_3 deposition. Both sides of free-standing graphene were covered with Al_2O_3 film during ALD deposition, as shown schematically in Figure 1a. A full coverage of Al_2O_3 films over graphene was achieved for thicknesses greater than 2.2 nm (20C-Al_2O_3@G), as shown in Figure S1. Samples of 1.1 and 2.2 nm thick revealed a nearly full coverage with some discontinuities still visible (Figure S1). The structures of all Al_2O_3 films were revealed to be amorphous according to the TEM diffraction patterns (Figure S1).

Quasi-static AFM deflection testing was first conducted to investigate the elastic and fracture responses of the films with different thicknesses (details in SI section 3). As shown schematically in Figure 1b, the center of the free-standing films was loaded to 100 nN for elastic studies and then to fracture for failure studies of a-Al_2O_3@G films (see SI section 4 for details). The elastic responses of all a-Al_2O_3@G films were consistent and repeatable with no significant hysteresis between loading−unloading curves. The elastic data of at least ten samples were collected for each film thickness and the representative force−film deflection ($F-\delta$) curves for a-Al_2O_3@G films, including pure CVD graphene, are shown in Figure 1c. It is evident that the mechanical stiffness increases with increasing thickness. The elastic moduli (E) of 10C-, 20C-, 30C-, 50C-, 100C-, 150C-Al_2O_3@G, and graphene were calculated as 294 ± 27, 207 ± 23, 176 ± 9, 174 ± 9, 168 ± 11, 163 ± 4, and 390 ± 34 GPa, respectively (see SI section 5 for details). Elastic modulus as a function of thickness was shown in Figure 1d, which reveals a ~55% decrease when increasing the thickness from 1.1 to 16.5 nm. A similar thickness dependency of E was reported for the free-standing ALD alumina films.[38,39] The elastic moduli for free-standing thin ALD alumina in literature were summarized in Table S1 with an average value of 166 GPa for films of 5−200 nm thick. The elastic moduli of 10C- and 20C-Al_2O_3@G was higher than thicker films and deviated from a rule-of-mixtures (ROM) analysis, likely due to a noncontinuous coverage of Al_2O_3 where graphene acted as the primary load-bearing component. Similar modulus reinforcement effect was observed for nonfully covered TiO_2@G films.[40] Further increasing the thickness continues to reduce the elastic modulus in a more gradual manner, and a plateau was further reached (after 30C-Al_2O_3@G) converging to the property of bulk amorphous alumina (within 6%), which demonstrates the minimal impact of the graphene layer on the modulus of a-Al_2O_3@G composites once the total thickness is above ~3.3 nm.

The static fracture behavior of a-Al_2O_3@G films was investigated by loading the center of the film until failure. The failure was identified by an abrupt force drop beyond 20% of the maximum force ($F_{Fracture}$).[44,45] Representative $F-\delta$ curves up to failure were provided in Figure S3. Figure 2a reveals the fracture force and toughness (energy-to-failure) normalized by the total film thickness, where a reduction of

https://dx.doi.org/10.1021/acs.nanolett.0c03868
Nano Lett. 2021, 21, 437−444

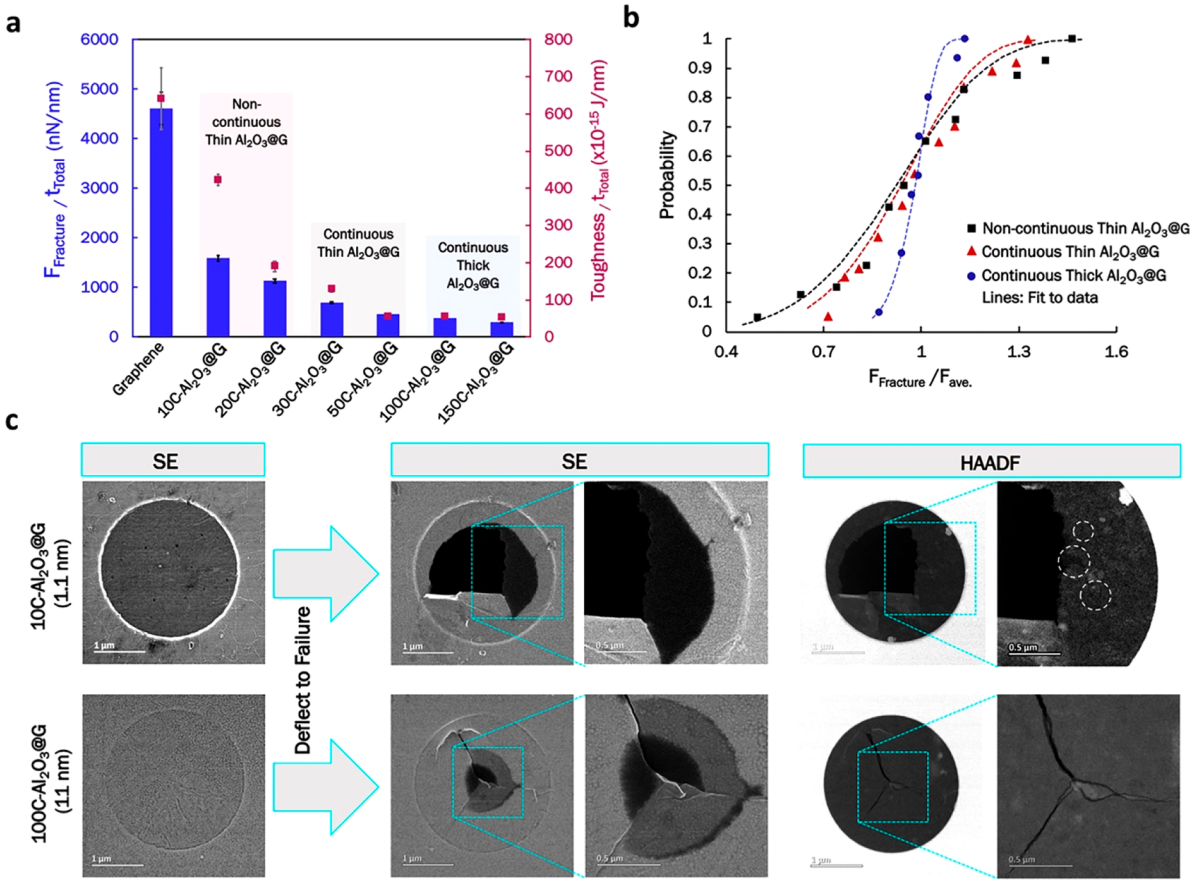

Figure 2. (a) Influence of film thickness on normalized fracture force and normalized toughness for all a-Al_2O_3@G films. The normalization is conducted by the thickness of a-Al_2O_3@G films. Highlighted sections refer to three groups of films based on thickness and film coverage. (b) Two-parameter cumulative Weibull probability distribution of the failure force of three groups a-Al_2O_3@G films with different thickness range and film coverage on graphene. (c) SE and HAADF images of 10C- and 100C-Al_2O_3@G before and after deflection to failure. White circles highlight the discontinuity in the 10C-Al_2O_3@G film.

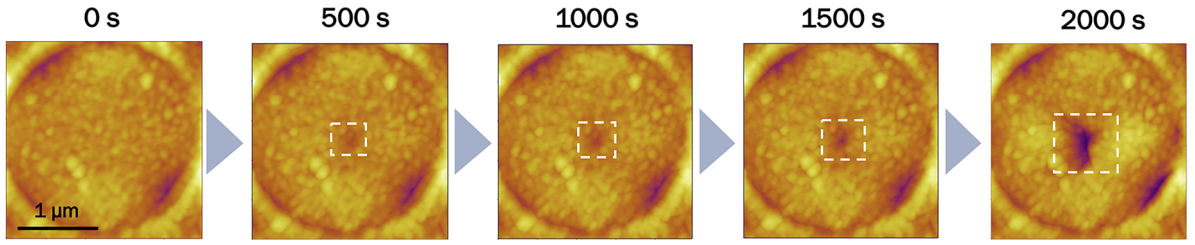

Figure 3. AFM topography images of 100C-Al_2O_3@G film after static dwelling up to 2000 s showing progressive plastic damage.

~81% and ~87% was achieved respectively when film thickness increases from 1.1 to 16.5 nm (10C- to 150C-Al_2O_3@G). We chose to report the fracture force rather than stress due to the complex stress state in the composite nanolayer. The effective averaged stress at the loading point of the films was also estimated using a continuum model (SI section 7 and Table S2) and showed ~70% strength reduction when thickness increases from 1.1 to 16.5 nm. A more detailed stress distribution near the indenter has also been modeled by finite element analysis (Figure S4). The trend of decreasing strength and normalized toughness also reached a plateau after 30C-Al_2O_3@G, where the ALD Al_2O_3 fully covers the graphene. A Weibull analysis[46] was performed in Figure 2b (details in SI section 8), which reveals a larger scatter in fracture force for thin films (both noncontinuous and continuous thin films) than (continuous) thick films. A higher scatter in the results typically indicates a higher sensitivity to the defects. Thinner films are expected to be more sensitive because any defects will be more detrimental to thinner samples than the thicker ones. Similar to the elastic properties, the fracture force and energy-to-failure of thinner films were more significantly affected by the graphene layer, and the behavior of Al_2O_3 films becomes more dominant after forming a continuous film over graphene.

Secondary electron (SE) and high-angle annular dark-field (HAADF) images of the fracture surface for 10C- and 100C-Al_2O_3@G samples in Figure 2c revealed significant differences. The 10C-Al_2O_3@G was found to fail catastrophically with film rupture, while 100C−Al_2O_3@G exhibited localized crack formation under the tip apex and crack propagation toward the edges. The failure morphology in Figure 2c suggests that during the fracture propagation process, the strain energy in

https://dx.doi.org/10.1021/acs.nanolett.0c03868
Nano Lett. 2021, 21, 437−444

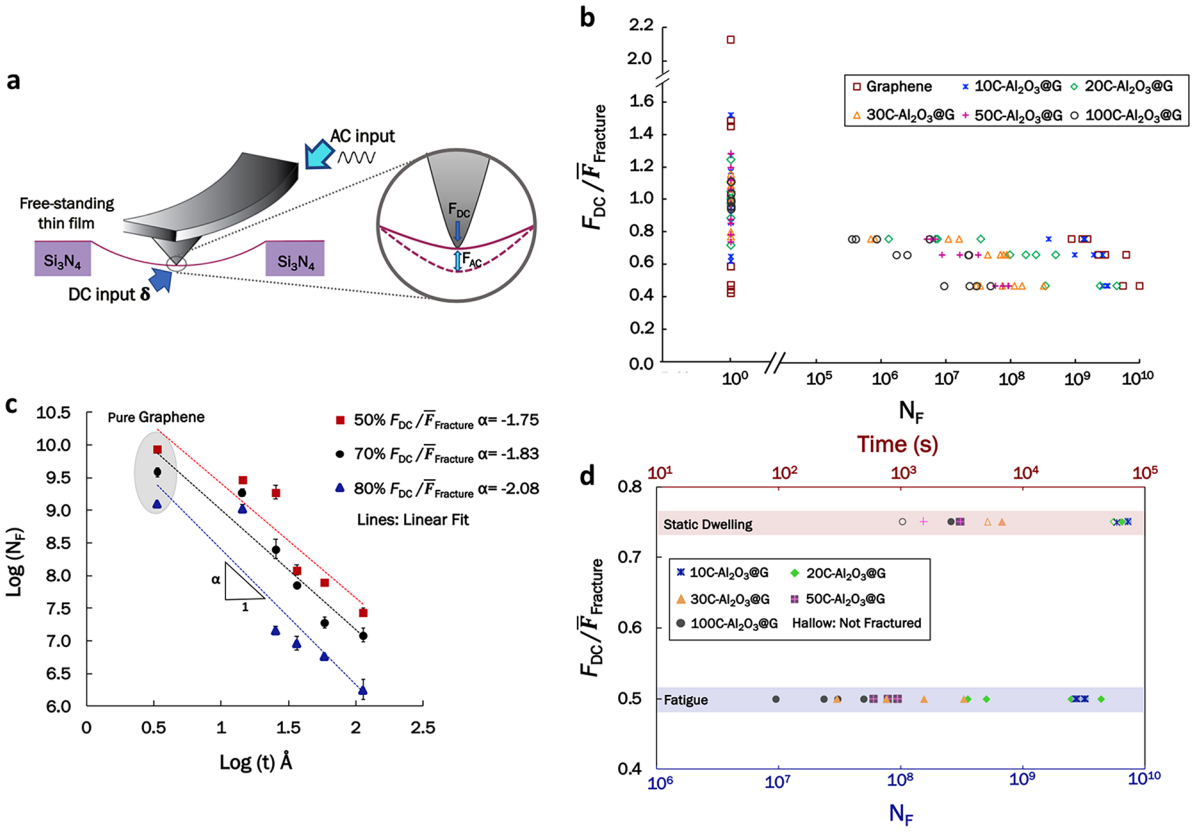

Figure 4. (a) Schematic of fatigue testing with F_{DC} and F_{AC} applied to the film center at the same time. (b) $F_{DC}/\bar{F}_{Fracture}$–$N$ curve of CVD graphene and a-Al_2O_3@G films showing a longer lifetime for lower DC force and smaller thicknesses. Note that the measured lifetime has an error within 1 s, equivalent to 1 × 10^5 cycles. (c) Average fatigue cycle number of a-Al_2O_3@G films at different force levels indicating thickness dependency of fatigue. Error bars represent the standard error of at least three sample measurements. (d) Comparison of lifetime between fatigue loading and static dwelling of a-Al_2O_3@G. Samples failed earlier under cyclic loading even though at a lower stress level.

thicker films can be released by forming through-thickness cracks while, on the contrary, the thinner films release the energy by forming more in-plane cracks that cause film rupture and delamination. Failure of amorphous alumina films at the nanoscale has been reported to be brittle;[27−31] however, several recent studies reported plastic deformation for alumina films of 50 and 35 nm thick.[32,33] Herein, deviations from linear behavior and minor force drops were evident in the failure F–δ curves of the 50C-, 100C-, and 150C-Al_2O_3@G films immediately before failure, which was highlighted in Figure S6. These deviations from linearity were likely due to the yield and initiation of plastic deformation at high forces just before the major fracture.

To further understand the potential plasticity, we performed a long-term static dwelling test. The center of the films was loaded to 85% of the average static failure force and maintained for a prolonged period, equivalent to a constant-load creep test. As shown in Figure 3, surface changes were evident after 1000 s of dwelling (highlighted in a white square), and significant local plastic damage was observed after 1500 s, although no sign of global failure was detected. The dwelling continued for another 500 s, and the size of the plastic damage zone increased. The plastic damage zone is more visible for thick films, such as 100C-Al_2O_3@G samples where there is a larger volume of alumina available for permanent deformation so that the cumulative damage is large enough to be detected. In the case of 30C-, 50C-Al_2O_3@G films, the damage was observed after 1 h of a dwelling, but the damage zone was smaller than thicker samples, which is due to the limited space (geometrical confinement) for creep diffusion activities,[47] and the damage could also be easily exhausted at the surface. Since graphene has been demonstrated with no measurable plastic behavior,[36] our results directly proved that viscous creep is a major mechanism for the plasticity of a-Al_2O_3 films. In addition, for the very thin a-Al_2O_3@G films, the supporting graphene layer with extremely high intrinsic strength could constrain and therefore hinder the plastic flow in alumina, resembling the blocking of dislocation movements at metal–graphene interfaces.[48]

2. Fatigue Fracture Behavior. Fatigue testing of a-Al_2O_3@G was conducted using a modified AFM technique reported in our previous study,[36] which enabled combined static and cyclic mechanical loading to nanofilms, which are schematically shown in Figure 4a (details in SI section 10). The fatigue tests were conducted for 10C-, 20C-, 30C-, 50C-, and 100C-Al_2O_3@G films as well as CVD monolayer graphene to investigate the effect of alumina film thickness and graphene support layer on the fatigue life (number of cycles to failure, N_F). Fatigue characterization of a-Al_2O_3@G films was conducted at varying static force (F_{DC}) levels equivalent to 80%, 70%, and 50% of the average fracture forces ($\bar{F}_{Fracture}$) for different thicknesses. In our previous study,[36] increasing the stress amplitude was shown to lower the N_F for graphene. In this work, a constant force range ΔF = 90 nN (equivalent to 1 nm of our cantilever oscillation amplitude, cantilever stiffness k = 45 N/m) was applied for all tests to focus on the mean force

https://dx.doi.org/10.1021/acs.nanolett.0c03868
Nano Lett. 2021, 21, 437−444

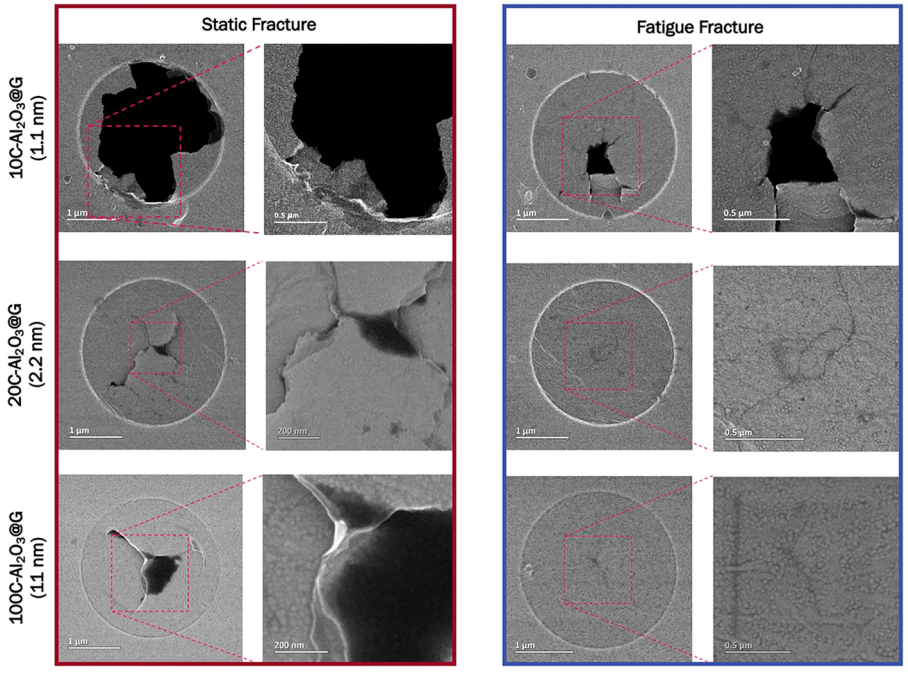

Figure 5. SE images comparing fracture morphology of 10C-, 20C-, and 100C-Al_2O_3@G films failed by static (left) and fatigue (right) loading.

effect on the fatigue life shown in Figure S7. The force−cycle (F−N) curves of a-Al_2O_3@G films and CVD graphene are shown in Figure 4b, and the static force in the vertical axis was normalized by the average static fracture force ($F_{DC}/\overline{F}_{Fracture}$). The data in N = 1 represent static loading to failure. For each specific thickness, the fatigue life increases with decreasing static force level. The F−N curve in Figure 4b also revealed a significant increase of N_F from 10^5 to 10^9 at 80% of $\overline{F}_{Fracture}$ when the alumina film thickness was reduced from 100C- to 10C-Al_2O_3@G (11.0 to 1.1 nm). A similar thickness effect was evident for fatigue tests under 70% of $\overline{F}_{Fracture}$ and 50% of $\overline{F}_{Fracture}$. The average N_F at different static force levels vs film thickness is plotted in Figure 4c, and a remarkable N_F was measured for all a-Al_2O_3@G films from millions to several billion cycles; meanwhile, a trend of reduced N_F with increasing thickness was also evident. The average N_F of CVD graphene (one to ten billion cycles under 50−80% of $\overline{F}_{Fracture}$) was at least 1 order of magnitude higher than that of a-Al_2O_3@G films. The high N_F for graphene was in a similar range reported for pristine graphene;[36] however, the stress amplitude applied here for CVD graphene is much lower than the tests conducted on pristine graphene. The N_F of 10C−Al_2O_3@G was in a range of a few billion cycles close to that of CVD graphene, which was attributed to the enhancement effect of graphene similar to that observed in the static behavior. The N_F of 30C-, 50C-, and 100C−Al_2O_3@G films was found to be reduced by two to 3 orders of magnitude. It is noted that stress amplitude should also be lower in thicker samples given the same applied cyclic force ΔF = 90 nN. The stress calculations based on a continuum model (details in SI sections 7 and 10) for graphene and a-Al_2O_3@G films (see Tables S3−S5) indicate that both the mean stress and stress amplitude decreases for thicker films. The fact that the thicker samples still having a shorter lifetime further confirms the significant size effect. However, if the film is too thick (e.g., >16.5 nm in this work), it turned out that the ΔF here would be below the fatigue threshold and cause little damage to the sample.

A comparison was made between fatigue loading and the long-term static dwelling to highlight the dynamic effect on the lifetime of the a-Al_2O_3@G films. Fatigue and dwelling tests were conducted at 50% and 75% of $\overline{F}_{Fracture}$, respectively. Under static dwelling, the samples were only subjected to ambient thermal fluctuations, which resulted in a near-zero (<20 pm) tip amplitude. As shown in Figure 4d, a-Al_2O_3@G films with different thicknesses could also fail under long-term static dwelling; however, the time-to-failure is at least twice longer than that under fatigue loading at even 50% of $\overline{F}_{Fracture}$. Therefore, it is clear that the cyclic loading could further contribute to a shorter lifetime of a-Al_2O_3@G films in addition to static loading. We attributed the significant cyclic effect to the viscous creep behavior of alumina (Figure 3), as well as the presence of the graphene/alumina interfaces, which involves severe energy dissipation during cyclic loading, especially at high loading frequencies such as 100 kHz in this work. Clear delamination at the alumina/graphene interface was observed only for samples under cyclic loading (Figure S9); meanwhile, for samples under static dwelling, the creep-induced fracture is the dominant failure mechanism.

The fracture morphology of a-Al_2O_3@G films failed under quasi-static (monotonic loading to failure) and fatigue loading (80% of $\overline{F}_{Fracture}$) was compared, and the fracture behavior also differs significantly for different thicknesses. As shown in Figure 5, the fracture morphology under quasi-static loading was catastrophic for 10C-Al_2O_3 films which were similar to the static failure of monolayer graphene, whereas the fatigue fracture caused more cracking and delamination, and less global rupture was evident. In contrast, 20C- and 100C-Al_2O_3@G exhibited cracks on the surface under fatigue loading in comparison to larger through-thickness holes under static loading. The fatigue behavior of a-Al_2O_3@G films shifted from graphene-dominated to alumina-dominated behavior with increasing thickness. Also, the thicker alumina films exhibited

https://dx.doi.org/10.1021/acs.nanolett.0c03868
Nano Lett. 2021, 21, 437−444

more plasticity under static loading, which contributes to the earlier failure under cyclic loading.

SUMMARY AND CONCLUSIONS

In this Letter, a systematic mechanics study, including elastic, static fracture, creep, and fatigue behavior of a-Al_2O_3@G nanofilms was investigatedusing AFM-based techniques. A single graphene layer was revealed to enhance the elastic, fracture, and fatigue life of a-Al_2O_3@G films up to a critical thickness of ∼3.3 nm, after which the intrinsic behavior of alumina was observed. Constant-load creep tests revealed obvious plasticity in a-Al_2O_3@G films, especially in films thicker than ∼3.3 nm; meanwhile, the plasticity in thinner films was hindered by the graphene layer and thus less evident. Fatigue testing also revealed a clear size-scale effect where a-Al_2O_3@G films of ∼1.1 nm thick could survive a few billion cycles (under $F_{DC}/\overline{F}_{Fracture}$ = 50%−80% and ΔF = 90 nN), which is up to 3 orders of magnitude higher than that of thicker (11 nm) a-Al_2O_3@G films. The observed plasticity in alumina and the presence of graphene/alumina interfaces were identified to contribute to the significant cyclic effect. The observed mechanical size effects (both static and fatigue properties) exhibited a shift from graphene-dominated to alumina-dominated behavior with increasing thickness. These results demonstrate the high static and dynamic reliability of ultrathin graphene-alumina nanolayers, and the mechanical enhancement effect of graphene, potentially guiding the optimal structural design in flexible optoelectronic devices.

It is noted that despite some existing challenges, significant progress on wafer-scale synthesis of high-quality graphene has been achieved,[49,50] and the roll-to-roll ALD processes have also shown great promise in large-scale industrial applications of various thin coatings.[51] The developed method could also be widely applied to other ultrathin nanolayers. It is anticipated that graphene may play a similar role in enhancing the fatigue life of other oxide glasses. Despite the fact that the absolute fatigue life is likely to be different for different material systems, a similar size effect may also exist. However, future studies including both experimental and atomistic simulations, are needed to investigate both the fatigue resistance and detailed mechanisms across different material systems.

ASSOCIATED CONTENT

Supporting Information

The Supporting Information is available free of charge at https://pubs.acs.org/doi/10.1021/acs.nanolett.0c03868.

Materials, STEM analysis, AFM measurements and calibration, static mechanical testing, elastic modulus calculation model, failure force−deflection curves of a-Al_2O_3@G films, stress calculation, Weibull distribution, failure behavior of thick a-Al_2O_3@G films, and fatigue testing (PDF)

AUTHOR INFORMATION

Corresponding Authors

Xueliang Sun − *Department of Mechanical and Materials Engineering, University of Western Ontario, London, Canada N6A 5B9*; Email: xsun9@uwo.ca

Tobin Filleter − *Department of Mechanical and Industrial Engineering, University of Toronto, Toronto, Canada M5S 3G8*; orcid.org/0000-0003-2609-4773; Email: filleter@mie.utoronto.ca

Authors

Maedeh Amirmaleki − *Department of Mechanical and Industrial Engineering, University of Toronto, Toronto, Canada M5S 3G8*; orcid.org/0000-0002-1206-930X

Teng Cui − *Department of Mechanical and Industrial Engineering, University of Toronto, Toronto, Canada M5S 3G8*; orcid.org/0000-0002-3218-2721

Yang Zhao − *Department of Mechanical and Materials Engineering, University of Western Ontario, London, Canada N6A 5B9*; orcid.org/0000-0002-4148-2603

Jason Tam − *Department of Materials Science and Engineering, University of Toronto, Toronto, Canada M5S 3E4*

Anukalp Goel − *Department of Mechanical and Industrial Engineering, University of Toronto, Toronto, Canada M5S 3G8*

Yu Sun − *Department of Mechanical and Industrial Engineering, University of Toronto, Toronto, Canada M5S 3G8*; orcid.org/0000-0001-7895-0741

Complete contact information is available at: https://pubs.acs.org/10.1021/acs.nanolett.0c03868

Author Contributions

†M.A. and T.C. contributed equally to this work.

Notes

The authors declare no competing financial interest.

ACKNOWLEDGMENTS

The authors acknowledge funding by the Natural Sciences and Engineering Research Council of Canada (NSERC), the Ontario Ministry of Research, Innovation, & Science, and the Erwin Edward Hart Professorship. ALD deposition was carried out at the Advanced Materials for Clean Energy Lab in the University of Western Ontario. STEM analysis was carried out at the Ontario Center for the Characterization of Advanced Materials (OCCAM).

REFERENCES

(1) Valant, M.; Luin, U.; Fanetti, M.; Mavrič, A.; Vyshniakova, K.; Siketić, Z.; Kalin, M. Fully Transparent Nanocomposite Coating with an Amorphous Alumina Matrix and Exceptional Wear and Scratch Resistance. *Adv. Funct. Mater.* **2016**, *26* (24), 4362−4369.

(2) Ogundare, F. O.; Olarinoye, I. O. He+ Induced Changes in the Surface Structure and Optical Properties of RF-Sputtered Amorphous Alumina Thin Films. *J. Non-Cryst. Solids* **2016**, *432*, 292−299.

(3) Aguilar-Gama, M. T.; Ramírez-Morales, E.; Montiel-González, Z.; Mendoza-Galván, A.; Sotelo-Lerma, M.; Nair, P. K.; Hu, H. Structure and Refractive Index of Thin Alumina Films Grown by Atomic Layer Deposition. *J. Mater. Sci.: Mater. Electron.* **2015**, *26* (8), 5546−5552.

(4) Katiyar, P.; Jin, C.; Narayan, R. J. Electrical Properties of Amorphous Aluminum Oxide Thin Films. *Acta Mater.* **2005**, *53* (9), 2617−2622.

(5) Daubert, J. S.; Hill, G. T.; Gotsch, H. N.; Gremaud, A. P.; Ovental, J. S.; Williams, P. S.; Oldham, C. J.; Parsons, G. N. Corrosion Protection of Copper Using Al2O3, TiO2, ZnO, HfO2, and ZrO2 Atomic Layer Deposition. *ACS Appl. Mater. Interfaces* **2017**, *9* (4), 4192−4201.

(6) Correa, G. C.; Bao, B.; Strandwitz, N. C. Chemical Stability of Titania and Alumina Thin Films Formed by Atomic Layer Deposition. *ACS Appl. Mater. Interfaces* **2015**, *7* (27), 14816−14821.

(7) Maydannik, P. S.; Kääriäinen, T. O.; Lahtinen, K.; Cameron, D. C.; Söderlund, M.; Soininen, P.; Johansson, P.; Kuusipalo, J.; Moro, L.; Zeng, X. Roll-to-Roll Atomic Layer Deposition Process for Flexible

Electronics Encapsulation Applications. *J. Vac. Sci. Technol., A* **2014**, *32* (5), No. 051603.
(8) Puurunen, R. L.; Saarilahti, J.; Kattelus, H. Implementing ALD Layers in MEMS Processing. *ECS Trans.* **2007**, *11* (7), 3−14.
(9) Finch, D. S.; Oreskovic, T.; Ramadurai, K.; Herrmann, C. F.; George, S. M.; Mahajan, R. L. Biocompatibility of Atomic Layer-Deposited Alumina Thin Films. *J. Biomed. Mater. Res., Part A* **2008**, *87* (1), 100−106.
(10) Zhao, Y.; Zheng, K.; Sun, X. Addressing Interfacial Issues in Liquid-Based and Solid-State Batteries by Atomic and Molecular Layer Deposition. *Joule* **2018**, *2* (12), 2583−2604.
(11) Klumbies, H.; Schmidt, P.; Hähnel, M.; Singh, A.; Schroeder, U.; Richter, C.; Mikolajick, T.; Hoßbach, C.; Albert, M.; Bartha, J. W.; et al. Thickness Dependent Barrier Performance of Permeation Barriers Made from Atomic Layer Deposited Alumina for Organic Devices. *Org. Electron.* **2015**, *17*, 138−143.
(12) Li, X.; Liu, J.; Meng, X.; Tang, Y.; Banis, M. N.; Yang, J.; Hu, Y.; Li, R.; Cai, M.; Sun, X. Significant Impact on Cathode Performance of Lithium-Ion Batteries by Precisely Controlled Metal Oxide Nanocoatings via Atomic Layer Deposition. *J. Power Sources* **2014**, *247*, 57−69.
(13) Li, X.; Liu, J.; Wang, B.; Banis, M. N.; Xiao, B.; Li, R.; Sham, T. K.; Sun, X. Nanoscale Stabilization of Li-Sulfur Batteries by Atomic Layer Deposited Al2O3. *RSC Adv.* **2014**, *4* (52), 27126−27129.
(14) Zhao, Y.; Amirmaleki, M.; Sun, Q.; Zhao, C.; Codirenzi, A.; Goncharova, L. V.; Wang, C.; Adair, K.; Li, X.; Yang, X.; et al. Natural SEI-Inspired Dual-Protective Layers via Atomic/Molecular Layer Deposition for Long- Life Metallic Lithium Anode Natural SEI-Inspired Dual-Protective Layers via Atomic/Molecular Layer Deposition for Long-Life Metallic Lithium Anode. *Matter* **2019**, *1* (Mld), 1−17.
(15) Castro Neto, A. H.; Guinea, F.; Peres, N. M. R.; Novoselov, K. S.; Geim, A. K. The Electronic Properties of Graphene. *Rev. Mod. Phys.* **2009**, *81* (1), 109−162.
(16) Balandin, A. A. Thermal Properties of Graphene and Nanostructured Carbon Materials. *Nat. Mater.* **2011**, *10* (8), 569−581.
(17) Falkovsky, L. A. Optical Properties of Graphene. *J. Phys. Conf. Ser.* **2008**, *129*, No. 012004.
(18) Lee, C.; Wei, X.; Kysar, J. W.; Hone, J. Measurement of the Elastic Properties and Intrinsic Strength of Monolayer Graphene. *Science* **2008**, *321* (5887), 385−388.
(19) Chen, W.; Gui, X.; Liang, B.; Yang, R.; Zheng, Y.; Zhao, C.; Li, X.; Zhu, H.; Tang, Z. Structural Engineering for High Sensitivity, Ultrathin Pressure Sensors Based on Wrinkled Graphene and Anodic Aluminum Oxide Membrane. *ACS Appl. Mater. Interfaces* **2017**, *9* (28), 24111−24117.
(20) Zhang, Y.; Li, X. Bioinspired, Graphene/Al2O3 Doubly Reinforced Aluminum Composites with High Strength and Toughness. *Nano Lett.* **2017**, *17* (11), 6907−6915.
(21) Rammula, R.; Aarik, L.; Kasikov, A.; Kozlova, J.; Kahro, T.; Matisen, L.; Niilisk, A.; Alles, H.; Aarik, J. Atomic Layer Deposition of Aluminum Oxide Films on Graphene. *IOP Conf. Ser.: Mater. Sci. Eng.* **2013**, *49* (1), 012014.
(22) Williams, J. R.; DiCarlo, L.; Marcus, C. M. Quantum Hall Effect in a Gate-Controlled p-n Junction of Graphene. *Science* **2007**, *317* (5838), 638−641.
(23) Vervuurt, R. H. J.; Kessels, W. M. M. E.; Bol, A. A. Atomic Layer Deposition for Graphene Device Integration. *Adv. Mater. Interfaces* **2017**, *4* (18), 1700232.
(24) Sangwan, V. K.; Jariwala, D.; Filippone, S. A.; Karmel, H. J.; Johns, J. E.; Alaboson, J. M. P.; Marks, T. J.; Lauhon, L. J.; Hersam, M. C. Quantitatively Enhanced Reliability and Uniformity of High-κ Dielectrics on Graphene Enabled by Self-Assembled Seeding Layers. *Nano Lett.* **2013**, *13* (3), 1162−1167.
(25) Wei, W.; Pallecchi, E.; Haque, S.; Borini, S.; Avramovic, V.; Centeno, A.; Amaia, Z.; Happy, H. Mechanically Robust 39 GHz Cut-off Frequency Graphene Field Effect Transistors on Flexible Substrates. *Nanoscale* **2016**, *8* (29), 14097−14103.
(26) Schijve, J. Fatigue of Structures and Materials in the 20th Century and the State of the Art. *Int. J. Fatigue* **2003**, *25* (8), 679−702.
(27) Munther, M.; Shaygan, M.; Centeno, A.; Neumaier, D.; Zurutuza, A.; Momeni, K.; Davami, K. Probing the Mechanical Properties of Vertically-Stacked Ultrathin Graphene/Al 2 O 3 Heterostructures. *Nanotechnology* **2019**, *30* (18), 185703.
(28) Mercier, D.; Mandrillon, V.; Parry, G.; Verdier, M.; Estevez, R.; Bréchet, Y.; Maindron, T. Investigation of the Fracture of Very Thin Amorphous Alumina Film during Spherical Nanoindentation. *Thin Solid Films* **2017**, *638*, 34−47.
(29) Berdova, M.; Ylitalo, T.; Kassamakov, I.; Heino, J.; Törmä, P. T.; Kilpi, L.; Ronkainen, H.; Koskinen, J.; Hæggström, E.; Franssila, S. Mechanical Assessment of Suspended ALD Thin Films by Bulge and Shaft-Loading Techniques. *Acta Mater.* **2014**, *66*, 370−377.
(30) van der Rest, A.; Idrissi, H.; Henry, F.; Favache, A.; Schryvers, D.; Proost, J.; Raskin, J. P.; Van Overmeere, Q.; Pardoen, T. Mechanical Behavior of Ultrathin Sputter Deposited Porous Amorphous Al2O3 Films. *Acta Mater.* **2017**, *125* (2017), 27−37.
(31) Jen, S. H.; Bertrand, J. A.; George, S. M. Critical Tensile and Compressive Strains for Cracking of Al2O3 Films Grown by Atomic Layer Deposition. *J. Appl. Phys.* **2011**, *109* (8), 084305.
(32) Frankberg, E. J.; Kalikka, J.; Garcia Ferré, F.; Joly-Pottuz, L.; Salminen, T.; Hintikka, J.; Hokka, M.; Koneti, S.; Douillard, T.; Le Saint, B.; et al. Highly Ductile Amorphous Oxide at Room Temperature and High Strain Rate. *Science* **2019**, *366* (6467), 864−869.
(33) Esmaeily, A. S.; Mills, S.; Coey, J. M. D. Exceptional Room-Temperature Plasticity in Amorphous Alumina Nanotubes Fabricated by Magnetic Hard Anodisation. *Nanoscale* **2017**, *9* (16), 5205−5211.
(34) Baumert, E. K.; Theillet, P. O.; Pierron, O. N. Fatigue-Resistant Silicon Films Coated with Nanoscale Alumina Layers. *Scr. Mater.* **2011**, *65* (7), 596−599.
(35) Baumert, E. K.; Pierron, O. N. Fatigue Properties of Atomic-Layer-Deposited Alumina Ultra-Barriers and Their Implications for the Reliability of Flexible Organic Electronics. *Appl. Phys. Lett.* **2012**, *101* (25), 251901.
(36) Cui, T.; Mukherjee, S.; Sudeep, P. M.; Colas, G.; Najafi, F.; Tam, J.; Ajayan, P. M.; Singh, C. V.; Sun, Y.; Filleter, T. Fatigue of Graphene. *Nat. Mater.* **2020**, *19*, 405−411.
(37) George, S. M. Atomic Layer Deposition: An Overview. *Chem. Rev.* **2010**, *110* (1), 111−131.
(38) Berdova, M.; Ylivaara, O. M. E.; Rontu, V.; Törmä, P. T.; Puurunen, R. L.; Franssila, S. Fracture Properties of Atomic Layer Deposited Aluminum Oxide Free-Standing Membranes. *J. Vac. Sci. Technol., A* **2015**, *33* (1), No. 01A106.
(39) Rontu, V.; Nolvi, A.; Hokkanen, A.; Haeggström, E.; Kassamakov, I.; Franssila, S. Elastic and Fracture Properties of Free-Standing Amorphous ALD Al 2 O 3 Thin Films Measured with Bulge Test. *Mater. Res. Express* **2018**, *5* (4), No. 046411.
(40) Cao, C.; Mukherjee, S.; Liu, J.; Wang, B.; Amirmaleki, M.; Lu, Z.; Howe, J. Y.; Perovic, D.; Sun, X.; Singh, C. V.; et al. Role of Graphene in Enhancing the Mechanical Properties of TiO2/Graphene Heterostructures. *Nanoscale* **2017**, *9*, 11678−11684.
(41) Wang, L.; Travis, J. J.; Cavanagh, A. S.; Liu, X.; Koenig, S. P.; Huang, P. Y.; George, S. M.; Bunch, J. S. Ultrathin Oxide Films by Atomic Layer Deposition on Graphene. *Nano Lett.* **2012**, *12* (2), 3706−3710.
(42) Purkl, F.; Daus, A.; English, T. S.; Provine, J.; Feyh, A.; Urban, G.; Kenny, T. W. Measurement of Young's Modulus and Residual Stress of Atomic Layer Deposited Al 2 O 3 and Pt Thin Films. *J. Micromech. Microeng.* **2017**, *27* (8), No. 085008.
(43) Tripp, M. K.; Stampfer, C.; Miller, D. C.; Helbling, T.; Herrmann, C. F.; Hierold, C.; Gall, K.; George, S. M.; Bright, V. M. The Mechanical Properties of Atomic Layer Deposited Alumina for Use in Micro- and Nano-Electromechanical Systems. *Sens. Actuators, A* **2006**, *130−131*, 419−429.
(44) Cui, T.; Mukherjee, S.; Cao, C.; Sudeep, P. M.; Tam, J.; Ajayan, P. M.; Singh, C. V.; Sun, Y.; Filleter, T. Effect of Lattice Stacking

https://dx.doi.org/10.1021/acs.nanolett.0c03868
Nano Lett. 2021, 21, 437−444

Orientation and Local Thickness Variation on the Mechanical Behavior of Few Layer Graphene Oxide. *Carbon* **2018**, *136*, 168−175.
(45) Amirmaleki, M.; Cao, C.; Wang, B.; Zhao, Y.; Cui, T.; Tam, J.; Sun, X.; Sun, Y.; Filleter, T. Nanomechanical Elasticity and Fracture Studies of Lithium Phosphate (LPO) and Lithium Tantalate (LTO) Solid-State Electrolytes. *Nanoscale* **2019**, *11* (40), 18730−18738.
(46) Lawn, B. *Fracture of Brittle Solids*, 2nd ed.; Cambridge University Press: Cambridge, U.K., 1993.
(47) Frankberg, E. J. Plastic Deformation of Amorphous Aluminium Oxide. *Doctoral Thesis*; Tampere University of Technilogy: Tampere, Finland, 2018.
(48) Kim, Y.; Lee, J.; Yeom, M. S.; Shin, J. W.; Kim, H.; Cui, Y.; Kysar, J. W.; Hone, J.; Jung, Y.; Jeon, S. Strengthening Effect of Single-Atomic-Layer Graphene in Metal-Graphene Nanolayered Composites. *Nat. Commun.* **2013**, *4*, 2114.
(49) Jiang, B.; Zhao, Q.; Zhang, Z.; Liu, B.; Shan, J.; Zhao, L.; Rümmeli, M. H.; Gao, X.; Zhang, Y.; Yu, T.; et al. Batch Synthesis of Transfer-Free Graphene with Wafer-Scale Uniformity. *Nano Res.* **2020**, *13* (6), 1564−1570.
(50) Grachova, Y.; Vollebregt, S.; Lacaita, A. L.; Sarro, P. M. High Quality Wafer-Scale CVD Graphene on Molybdenum Thin Film for Sensing Application. *Procedia Eng.* **2014**, *87*, 1501−1504.
(51) Ali, K.; Choi, K.-H.; Jo, J.; Lee, Y. W. High Rate Roll-to-Roll Atmospheric Atomic Layer Deposition of Al2O3 Thin Films towards Gas Diffusion Barriers on Polymers. *Mater. Lett.* **2014**, *136*, 90−94.

https://dx.doi.org/10.1021/acs.nanolett.0c03868
Nano Lett. 2021, 21, 437−444